



Experimental and modelling of the thermal regions of activity during pyrolysis of bituminous coals

Vladimir Strezov^{a,*}, John A. Lucas^b, Les Strezov^c

^a *Newbolds Applied Research, The University of Newcastle, Cnr Frith and Gavey Streets, Mayfield 2304, NSW, Australia*

^b *Discipline of Chemical Engineering, Faculty of Engineering and Built Environment, The University of Newcastle, University Drive, Callaghan 2308, NSW, Australia*

^c *Strezov Consulting, 7 Marin Street, Adamstown 2289, NSW, Australia*

Received 10 January 2003; accepted 6 June 2003

Abstract

Computer-aided thermal analysis technique, incorporated with thermogravimetric and Fourier transform infrared (TG–FTIR), and mass spectrometry, were employed in studying the devolatilisation of three thermal bituminous coals under packed bed pyrolysing conditions. The heats of reactions evolved during coal devolatilisation were determined by computational calorimetry and compared with the evolution rate of fourteen volatile species. The devolatilisation was classified into five major regions of thermal activity, according to the analysis, where the first was related to the dehydration of strongly bounded water. The second was the pre-plastic region with an endothermic prepyrolytic reaction, while the third was the exothermic plastic range with primarily evolution of tars and re-solidification reactions. The secondary devolatilisation was found to be endothermic and the major contributors were hydrocarbons, secondary water, CS₂ and H₂S. The largest reaction was the contraction of carbon planes with evolution of hydrogen. Each reaction region was assumed to follow the first-order Arrhenius kinetic correlation and the activation energy was determined for each of the five regions. The activation energies were then incorporated into a simplified model for predicting the overall heats of reactions.

© 2003 Elsevier B.V. All rights reserved.

Keywords: Coal; Reactions; Thermal analysis; Gas analysis; Kinetics

* Corresponding author. Tel.: +61-2-4968-6771; fax: +61-2-4968-6777.
E-mail address: vladimir.strezov@newcastle.edu.au (V. Strezov).

1. Introduction

The thermal decomposition of coal is a complex phenomenon comprising of chemical and physical changes within the coal structure. The coal molecular bonds are ruptured upon heating where the weaker bonds start to break at lower temperatures and the stronger bonds at higher [1], evolving different gaseous species and continuously changing the coal macromolecular structure [2]. Gaseous products predominantly contain oxides of carbon, hydrocarbons, hydrogen and tars. Coal decomposition has been previously considered as a three-stage process [3], where during the first stage it undergoes bond breaking, melting and formation of metaplast. The metaplast is a plastic liquid, which during the second stage, decomposes upon heating, forming char and evolving tars and primary gases. The temperature at which the plastic material is eliminated from the structure is termed as re-solidification. During the third stage, gaseous products continue to react evolving secondary gases, while undergoing condensation of the carbon rings. Under moderate heating rates, coking coals form bubbles within the plastic phase and the pressure generated in the bubbles causes substantial swelling. Contrary to this behaviour, thermal coals with non-plastic properties maintain consistence of the open pore surface structure throughout the entire heating range, allowing free escape of the volatiles, with insignificant swelling [4]. Swelling properties of these coals change under flash pyrolysing conditions, with the swelling ratio being affected by the maceral constituents and mineral content represented in the coal [5].

Premium coking coals, due to their swelling properties can form coke. Coke is utilised in blast furnace operations providing energy and source of carbon for iron oxide reduction. Thermal coals became of an interest to the iron- and steel-making community with the recent developments of direct reduced iron (DRI) technologies. The DRI technology has the potential to eliminate coke-making and sintering processes and become a sustainable metallurgical operation [6]. At present, these processes are essential components at the front end of the conventional blast furnace iron-making technology, adding to the overall capital and operational cost of the plant and causing serious environmental concerns.

The DRI process consists of reduction of the iron oxide directly from volatiles, such as CO and H₂, liberated during coal devolatilisation, as well as carbon monoxide, regenerated according to the Boudouard reaction [7]. In this way, the reducing properties of the coal are enhanced and the iron-making process avoids the necessity for the use of premium coking coals. This generates an advanced utilisation opportunity for the high volatile thermal coals, which have long been considered as inappropriate for the steel industry [8]. Optimisation of the process, however, depends on the thermal behaviour of the coals under conditions of pyrolysis. Defining the thermal properties, including specific heat and enthalpy, thermal regions and the ability to predict the thermal behaviour of the coal pyrolysis is in this respect of great importance.

With the development of new iron-making and coal conversion technologies, characterisation of carbonisation becomes increasingly important. Understanding of the thermal behaviour of coal during pyrolysis, synergetic effects of additives and behaviour of coal in mixtures with iron ore, is required to help model and advance the engineering designs for these new technologies. Coals have been extensively thermally studied using differential methods of analysis. The results are rather contrary, with some authors reporting predominantly endothermic [9–11] while others only exothermic heats of coal reactions [12–14].

There are several possible reasons why the reports in the literature are conflicting. These include differences in the ranks of coals used in the analysis, different heating conditions and different final temperature of pyrolysis where devolatilisation reactions occurring at higher temperature have not been completed.

In this work, the authors have employed the computational calorimetric method in combination with gas analysis, to better define and understand the regions of activity during pyrolysis of thermal bituminous coals. The computational calorimetry is carried out by heating coal samples under defined heat transfer conditions and calculating the sample thermal properties by employing an inverse numerical technique. This method has a significant potential in the thermal analysis of materials, and the reported work herewith outlines its applications in studying coal devolatilisation.

2. Experimental

2.1. Samples

The analysis and rank of the coal samples selected for this study are shown in Table 1. The samples were ground to $\sim 212 \mu\text{m}$ and dried under vacuum at 80°C for 2 h prior to each experiment.

2.2. Computer-aided thermal analysis

Computer-aided thermal analysis was performed on three coal samples. The thermal analysis technique has been detailed elsewhere [15,16]. The following text presents a brief summary of this technique.

Table 1
Coal analysis and rank

	Baal Bone	Drayton	Moura
Proximate analysis (air dried)			
Fixed carbon (%)	55.8	50.1	58.6
Volatile matter (%)	32.2	37.7	31.6
Ash (%)	9.2	10.6	7.6
Moisture (%)	2.8	1.6	2.2
Ultimate analysis (dry and ash-free)			
Carbon (%)	84.1	82.7	83.4
Hydrogen (%)	5.16	5.98	5.19
Nitrogen (%)	1.92	1.81	1.93
Oxygen (%)	8.18	8.5	9.01
Sulphur (%)	0.64	0.97	0.47
ASTM rank	HVA	HVA	HVA
CSN	1	2.5	0.5
Gieseller plastometer			
Initial softening temperature	420	400	–
Maximum fluidity temperature	435	435	–
Maximum fluidity (ddpm)	5	15	<5
Re-solidification temperature	450	455	–

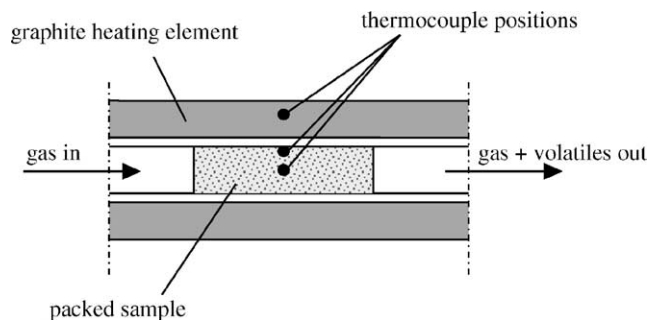


Fig. 1. Schematic diagram of the experimental set-up.

The coal sample, weighing 2.35 g, was packed inside the 10.6 mm i.d. quartz sample tube and insulated on the sides with alumina ceramics. The quartz glass tube was then covered with carbon soot on the outer surface to ensure uniform emissivity is achieved throughout the glass. The glass tube with the packed coal sample was located concentric to a graphite radiator, as shown in Fig. 1. The assembly was placed inside an infrared furnace and both the graphite and the sample tube were kept under inert atmosphere with separate flows of argon gas. The flow of argon gas through the sample ensured that volatiles developed by decomposition are promptly removed from the heated zone and prevented from oxidising the sample. The experimental set-up in this way simulates temperature controlled packed bed pyrolyser.

Three chromel–alumel thermocouples, 1 mm in diameter, were used during the measurements, one embedded inside the graphite tube and used to control the heating rate of the furnace set at 10 °C/min, and two thermocouples placed on the surface and in the centre of the sample. The temperature acquisition was conducted at 1 Hz logging rate and the data were stored in a computer. Thermal analysis was performed with the stored temperature data by applying an inverse modelling technique to solve the heat conduction Eq. (1):

$$C_p \frac{\partial T}{\partial t} = \nu k \frac{\partial}{\partial r} \left(r \frac{\partial T}{\partial r} \right) \quad (1)$$

where C_p is the specific heat (J/(kg K)), k the thermal conductivity (W/(m K)), ν the specific volume (m³/kg), T the temperature (K), t the time (s), and r is the radius (m).

The sample was divided in a grid pattern with a number of nodes n across the radius. The heat balance for each node was calculated based on the principle that the heat accumulated by the node equals the difference of the heat entered and heat released from the node. The fully implicit discretisation equation expressed in radial co-ordinates for this grid geometry is presented in Eq. (2):

$$\frac{2\pi \Delta x^2 i}{\Delta t k \nu} C_p (T_i^t - T_i^{t-1}) = 2\pi(i + \frac{1}{2})(T_{i+1}^t - T_i^t) - 2\pi(i - \frac{1}{2})(T_{i-1}^t - T_i^t) \quad (2)$$

where T_i^t is the temperature expressed in K for the node i at a time t .

The boundary conditions of the system were the temperatures measured at the centre and surface of the sample, zero heat flux in the centre of the sample and surface heat flux

calculated assuming radiative heat transfer from the graphite tube to the sample described by Eq. (3):

$$Q = F_{1-2} \sigma (T_g^4 - T_s^4) \quad (3)$$

where Q is the heat flux (W/m^2), σ the Stefan–Boltzmann constant, T_g the graphite temperature (K), T_s the sample surface temperature (K) and F_{1-2} is the radiation shape factor estimated through calibration as a function of the graphite temperature [15,16].

The computational matrix using Eq. (4) was developed for the estimate of the apparent specific heat of the heated material based on the initial mass of dried sample. For closer familiarisation with the equation evaluation procedure, see [15–18].

$$C_p = 2\pi n \Delta x \nu Q(t) \left[\frac{\Delta x^2 \pi}{4\Delta t} (T_0^t - T_0^{t-1}) + \frac{\Delta x^2 \pi}{\Delta t} (n - \frac{1}{4})(T_n^t - T_n^{t-1}) + \sum_{i=1}^{n-1} \frac{2\pi \Delta x^2 i}{\Delta t} (T_i^t - T_i^{t-1}) \right]^{-1} \quad (4)$$

2.3. Gas analysis

Thermogravimetric and Fourier transform infrared (TG–FTIR) analysis was used to measure weight loss and evolution of volatiles and tars during heating at $10^\circ\text{C}/\text{min}$. The

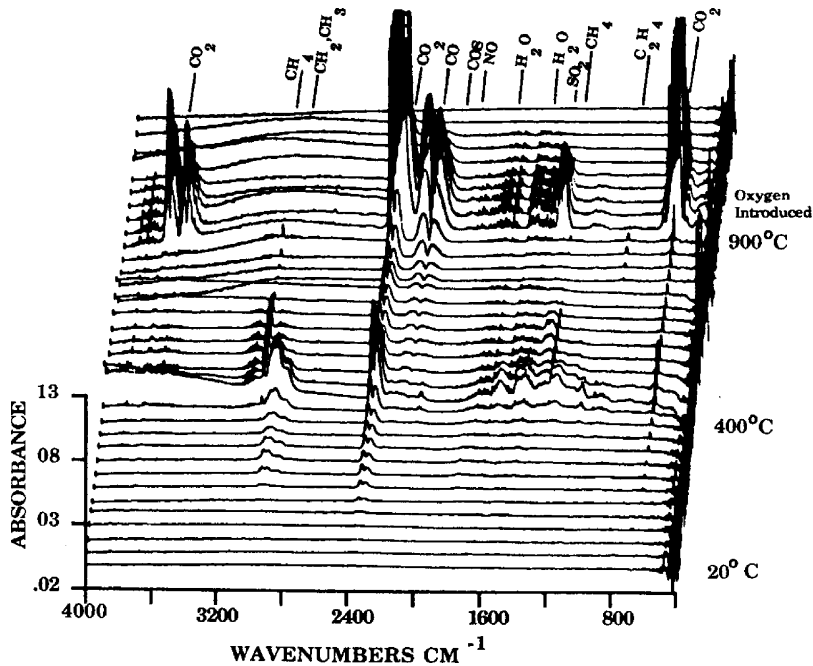


Fig. 2. TG–FTIR spectra of coal showing absorption bands of gaseous products [19].

apparatus and experimental procedure for this analysis were identical to the one described by Carangelo et al. [19]. The volatiles determined with TG–FTIR analysis were tars, CH₄, C₂H₄, CO, CO₂, H₂O, HCN, NH₃ and CS₂. Fig. 2 presents a series of spectra showing absorption bands for volatile species obtained during pyrolysis.

Some of the gaseous products undetected with the FTIR technique were analysed with a mass spectrometer. The mass spectrometer Prima 600 from VG Gas Analysis Systems was connected to the gas outlet of the glass sample tube. The sample surface and centre thermocouples were not used in this analysis in order to avoid any gas leakage from the thermocouple connections. Only the temperature of graphite tube was logged and used to calculate the temperature of sample. Logging of the mass spectrometric data was performed every 10 s. Volatile species determined with the mass spectrometric analysis were C₂H₆, C₃H₈, C₄H₁₀, H₂ and H₂S having mass numbers 30, 44, 58, 2 and 34, respectively.

3. Results

Fig. 3 shows comparison between the apparent and real specific heat of the three coals determined by computer-aided thermal analysis technique. The apparent specific heat incorporates the thermal reactions developed during the heating process. If energy is consumed, during an endothermic reaction, it is reflected in increased specific heat, while the exothermicity decreases the specific heat. Clearly, the apparent specific heat shows various thermal reactions taking place during pyrolysis. Separating the reaction regions and quantifying the reaction heats requires measurement of the real specific heat. The real specific heat was determined by producing an inert char for the temperatures of interest, in consecutive heating and cooling cycles, according to Tomeczek and Palugniok [20] and Agroskin et al. [21]. The sample was heated for a period of 4 h, cooled to room temperature and re-heated again at 10 °C/min up to the next temperature of interest, behaving as an inert char in the pre-heated region. The real specific heat was obtained in increments of about 100 °C. The difference between the apparent and the real specific heat gave the heats released during coal thermal decomposition.

Fig. 4 shows the extracted reactions of coal pyrolysis clearly exhibiting five distinctive regions of activity. In order to understand the reactions taking place in each region, volatile species developed during pyrolysis were analysed and presented in Figs. 5–7. Fourteen volatile species, including tars, were detected by using the two separate analytical methods.

Tars were released within the temperature range of 380–550 °C, where a dominant exothermic reaction was observed. The particular reaction of the release of tars is known to be endothermic. There is a very small endothermic peak appearing at 460 °C for Baal Bone and Drayton, which is related to the evolution of tars. Under moderate heating rates, however, this effect is insignificant and the endothermic tar release is masked by the overall exotherm. Moura did not exhibit significant changes in this region.

The evolution of methane appeared in the region where a large endothermic reaction occurred. The maximum evolution rate corresponded well with the endothermic peak. The ethylene evolution preceded the methane release in much smaller quantities. The maximum evolution of ethane, propane and butane appeared between 430 and 630 °C. In comparison with the heats of devolatilisation, the evolution rate fell between the exothermic and the

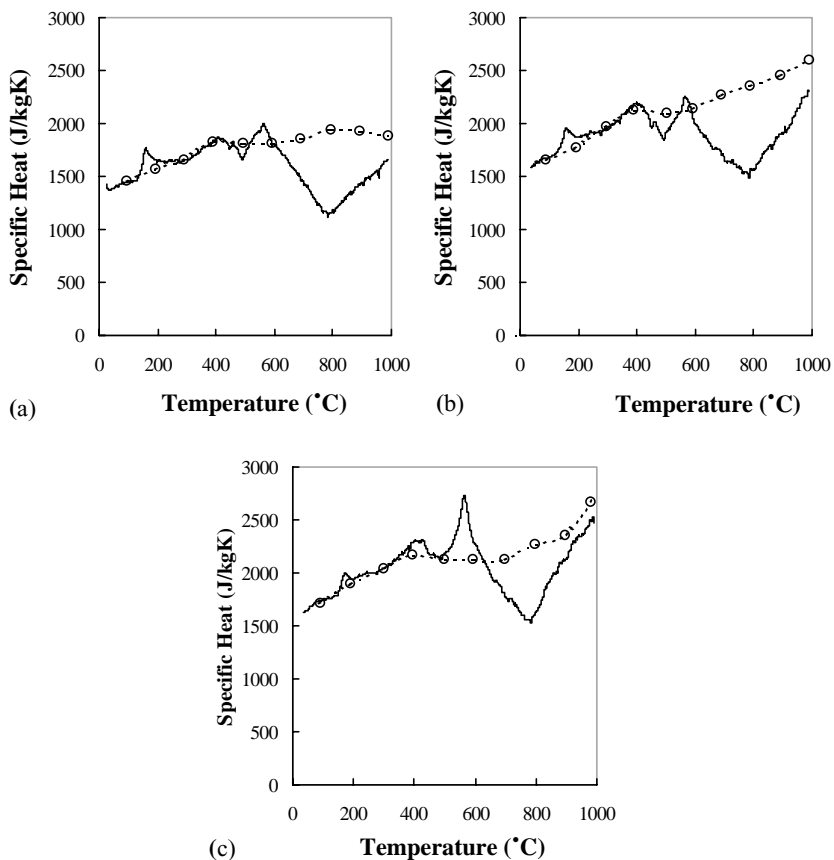


Fig. 3. Apparent (—) and real (○) specific heats: (a) Baal Bone; (b) Drayton; (c) Moura.

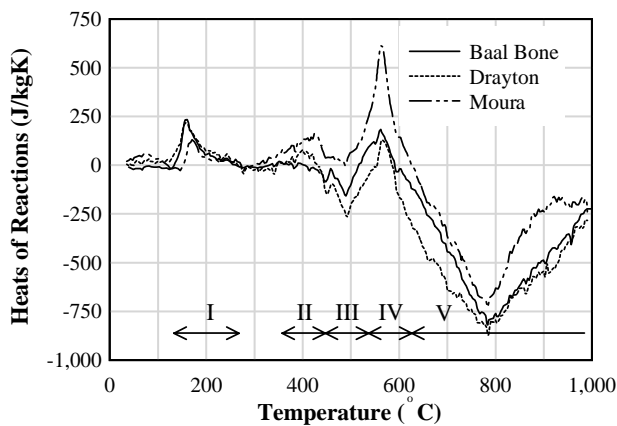


Fig. 4. Heats of reactions and regions of activity of coal devolatilisation.

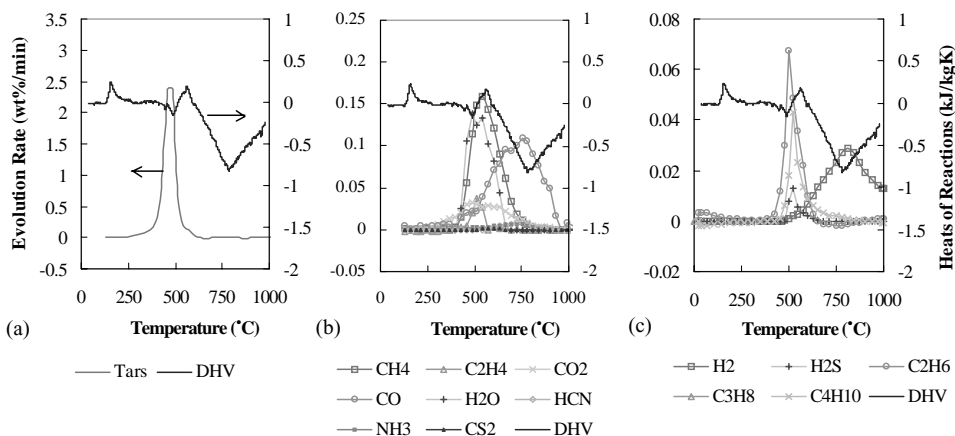


Fig. 5. Rate of evolution of volatile compound products from pyrolysis of Baal Bone superimposed to the measured heats of reactions: (a) rate of evolution of tars; (b) rate of evolution of volatiles determined by TG-FTIR analysis; (c) rate of evolution of volatiles determined by mass spectrometry.

endothermic reactions with peaks between 500 and 550 °C, with probably overall endothermic effect. The release of H₂O, CS₂ and H₂S appeared in the similar temperature regions with peaks between 500 and 600 °C. Their release could be related to the endothermic heat effect in this region.

The evolution of hydrogen commenced after 500 °C achieving a maximum around 800 °C. The profile of the curve was related to a large exothermic reaction, displaying maximum evolution at the same temperature where the exothermic trough appeared. The evolution

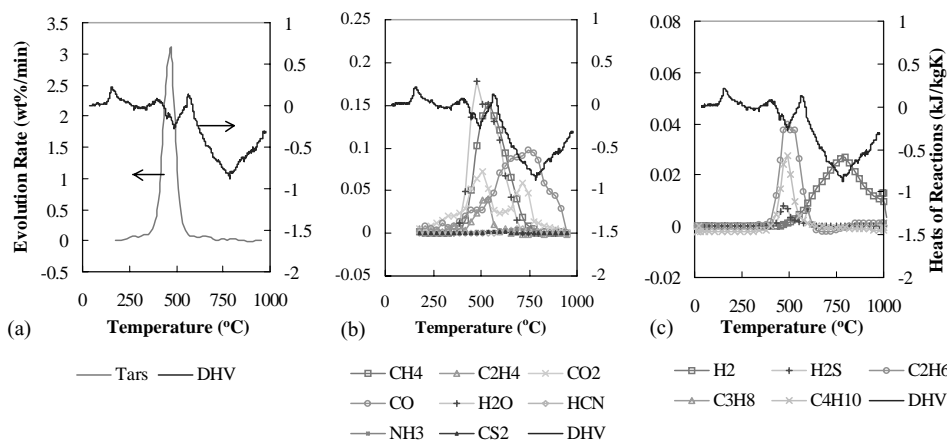


Fig. 6. Rate of evolution of volatile compound products from pyrolysis of Drayton superimposed to the measured heats of reactions: (a) rate of evolution of tars; (b) rate of evolution of volatiles determined by TG-FTIR analysis; (c) rate of evolution of volatiles determined by mass spectrometry.

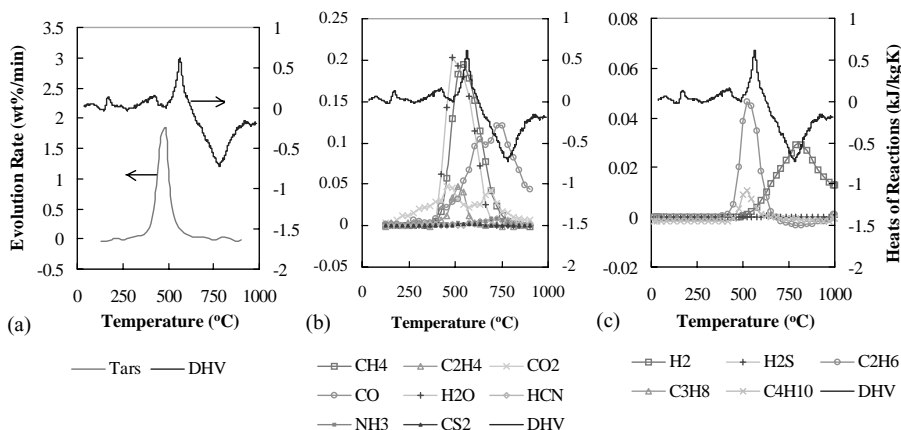


Fig. 7. Rate of evolution of volatile compound products from pyrolysis of Moura superimposed to the measured heats of reactions: (a) rate of evolution of tars; (b) rate of evolution of volatiles determined by TG-FTIR analysis; (c) rate of evolution of volatiles determined by mass spectrometry.

of CO showed similar profile as the hydrogen release. It also appeared in the exothermic region, after 400 °C with maximum rate of evolution at around 750 °C. The rate of CO₂ release exhibited two peaks, at 450 and around 700 °C, for all coal samples. The heat effects during CO₂ formation and release were most likely negligible and did not correspond to the heat changes. The evolution rate of NH₃ and HCN in all samples corresponded to the exothermic reaction above 600 °C. The shapes of the curves were similar with the evolution rates of H₂ and CO, exhibiting peaks between 700 and 750 °C.

Table 2 summarises temperatures where each volatile component starts to evolve, achieves maximum and completes the evolution. Some of the volatile species such as H₂, CO and CO₂ still evolved when the temperatures reached 1000 °C indicating that the devolatilisation process was not entirely completed by the end of the experiments.

4. Interpretation of the thermal regions

The first endothermic reaction was related to the release of water with a peak between 140 and 180 °C. As samples were first pre-dried, the water left in the samples was attributed to the stronger bonded water, which evolved between 110 and 150 °C. It should be noted that this water had no correlation with the water measured with the FTIR analysis, which was a product of the secondary reactions.

The amount of the water remaining in the dried sample was calculated using the measured energies, which were determined by integrating the curves in Fig. 4, while assuming 2.5 MJ/kg for the latent heat of water vaporisation. Calculated amounts were several times smaller than the moisture from the proximate analysis (see Table 1). This was due to the difference in the sample preparation procedure. In the present study, samples were dried under vacuum conditions while in the standard proximate analysis the samples were air-dried. The

Table 2
Summary of the evolution of gaseous species with respect to the various temperatures

Coal	T_{start}	T_{max}	T_{fin}	T_{start}	T_{max}	T_{fin}
		TARS			CH ₄	
BB	375	475	555	405	545	810
DR	375	475	555	405	550	780
MO	375	475	575	415	545	780
		C ₂ H ₄			C ₂ H ₆	
BB	445	525	575	430	515	630
DR	435	525	575	415	500	630
MO	435	535	600	440	540	660
		C ₃ H ₈			C ₄ H ₁₀	
BB	450	520	650	450	520	650
DR	405	495	575	405	495	590
MO	435	525	620	450	525	610
		H ₂			CO	
BB	500	810	–	395	750	–
DR	465	790	–	345	750	–
MO	500	810	–	400	720	–
		CO ₂			H ₂ O	
BB	280	475	860	395	475	680
DR	200	515, 723	–	365	485	690
MO	160	465, 680	–	395	485	710
		H ₂ S			NH ₃	
BB	480	520	670	415	720	880
DR	420	480, 595	640	435	690	850
MO	510	630	710	445	720	900
		HCN			CS ₂	
BB	555	760	–	515	585	720
DR	565	710	830	505	565	810
MO	555	700	870	485	555	740

T_{start} : temperature at which the volatile substances start to evolve; T_{max} : temperature at which the maximum is achieved, and T_{fin} : temperature at which the evolution is complete. All temperatures are expressed in degree Celcius.

moisture contents calculated from the heats of devolatilisation curves were compared with the contents obtained from the thermogravimetric analysis in Table 3, as the sample preparation was identical in both cases. The typical TGA curve for one coal sample, enlarged for the temperature region of water vaporisation, is presented in the Fig. 8. The water content calculated from the dehydration reaction was of the same order as the one determined from the TGA measurements.

The coal samples displayed an early endothermic reaction in region II, as shown in Fig. 4, with the peak at around 420 °C. This is the region where most coals typically undergo initial softening. Gaseous products analysed with FTIR and mass spectrometry did not detect any of the major gas species during this reaction. The origins of this endothermic effect could be attributed to the prepyrolytic physical transition reported by Yun and Suuberg [22]. This

Table 3
Comparisons of the amounts of water in the sample obtained by calculation from the heats of devolatilisation results and from the TGA

	$\Delta H_{V_{H_2O}}$ (kJ/kg)	Amount of water by calculation (% of original coal)	Amount of water from TGA data (% of original coal)
Baal Bone	13.4	0.6	0.4
Drayton	13.9	0.7	0.6
Moura	5.5	0.3	0.6

transition was found to be an irreversible structural relaxation taking place prior to the plastic thermal range.

All measured samples, with the exception of Moura, had an exothermic reaction in region III, with a trough located at 490 °C. This reaction, taking place in the plastic range, is related to the plastic properties and swelling of the coal. In this region, following completion of the softening process, coals melt forming metaplast and re-solidify as char. The melting process is believed to be endothermic, while re-solidification is an exothermic process [23]. Physical changes related to the plastic properties have an effect on the overall heat releases in this region. The release of heavy volatiles and tars is associated with endothermic reaction of bond breaking and tar vaporisation.

Following re-solidification, secondary devolatilisation commenced associated with endothermic reactions in region IV, having a peak at around 570 °C. Methane gas evolved in the same temperature range as the endothermic reaction peak. The evolution of other hydrocarbons, although exhibiting maximum rate at lower temperatures, could also be related to the endothermic secondary reactions. Other gaseous species, released in this region and associated with the endothermic secondary reactions, were the secondary water, CS₂ and H₂S.

A significant exotherm was monitored above 600 °C in region V (see Fig. 4). Although several gaseous species were detected in this temperature range, such as H₂, CO, NH₃ and

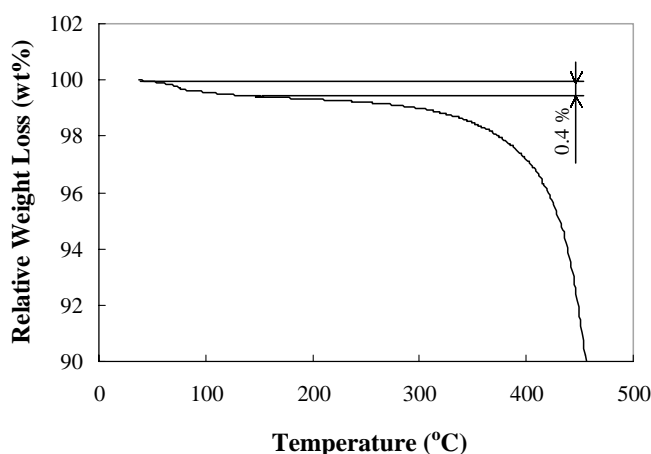


Fig. 8. Amount of water in Baal Bone estimated from the TGA data.

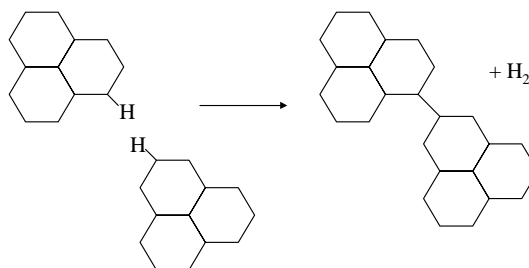


Fig. 9. Mechanism of hydrogen formation.

HCN, previous studies [10,24] suggested that this exotherm was mostly influenced by the release of hydrogen. According to Berkowitz and den Hertog [25], the formation of hydrogen is a bimolecular process occurring when two contiguous lamellae move into a configuration in which the chemical interaction between them becomes possible. The simplified mechanism of hydrogen formation and release is shown in Fig. 9. The C–H bonds break evolving hydrogen, reflecting the formation of stronger bonds between the carbon atoms. This is followed by condensation and contraction within the carbon hexagonal planes. The trough located around 790 °C, in Fig. 4, indicates the commencement of the graphitisation process.

Heats from each of the regions were calculated by integrating the curves in Fig. 4 and are summarised in Table 4. It is evident that the exothermic reaction in region V was by far greater than the heats from the previous regions. It has been reported that during coke-making the centre of the coke oven can become hotter than the heated layers closer to the oven walls [26]. These observations could be explained by the strong exothermal reaction taking place in the region V. The contraction reactions provide excess energy in the coal utilisation process and, as hydrogen and CO are mainly driven off at this stage, it is beneficial for the direct reduction of iron.

It is clear that besides being chemically driven, the contraction reaction is also a reflection of the physical changes. X-ray diffraction (XRD) is useful in obtaining the crystallite structure of materials. In the field of coal related studies, Davis et al. [27] applied this analysis in identifying the turbostatic crystallite dimensions in chars as a function of the temperature history. A similar approach was applied in this work in order to investigate the changes in the crystallite size of coal chars as a function of temperature.

Table 4
Regions of coal thermal activity defined by the reaction enthalpy

Coals	Region I (dehydration)		Region II (pre-plastic stage)		Region III (plastic stage)		Region IV (secondary devolatilisation)		Region V (contraction)	
	ΔH	E	ΔH	E	ΔH	E	ΔH	E	ΔH	E
Baal Bone	14.8	68	≈0	≈0	−9.4	124	10.0	335	−259	98
Drayton	15.4	80	3.6	144	−18.7	190	3.1	988	−275	95
Moura	6.1	103	15.5	74	≈0	≈0	37.9	157	−155	130

The heats of reactions ΔH are expressed in kJ/kg and activation energies E in kJ/mol.

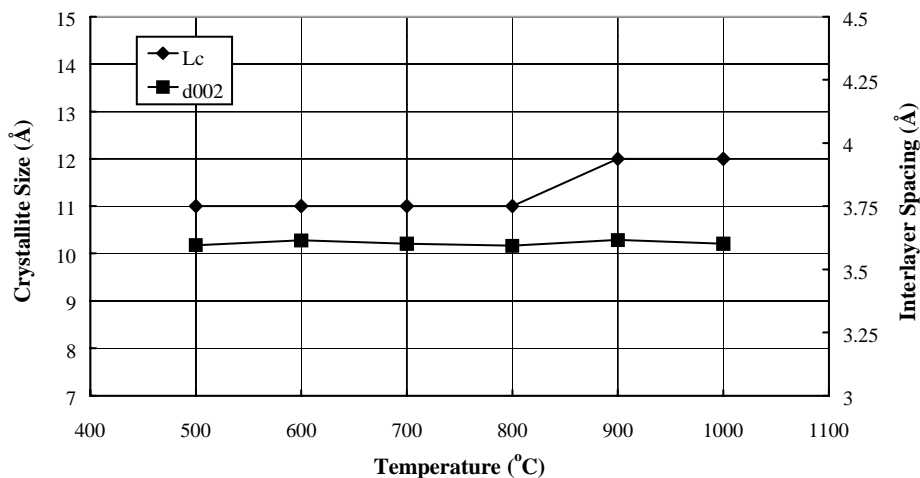


Fig. 10. Crystallite dimensions calculated from XRD spectra where L_c is the crystallite size and d_{002} interlayer spacing.

Char samples were prepared by preheating the Baal Bone sample at different temperatures in the region V for a period of 4 h. The XRD analysis was carried out on a SIEMENS D5000 X-ray diffractometer with monochromator and a Cu $K\alpha$ X-ray source. The interlayer spacing d_{002} was determined from the XRD trace ($d = \lambda/2 \sin \theta$) and the crystallite size L_c (Å) was calculated by using the Scherrer equation:

$$L_c = \frac{0.9\lambda}{B \cos \theta_B} \quad (5)$$

where L_c is the parallel layer group dimension normal to the layers, λ the wavelength of the incident X-ray ($\lambda = 1.5406 \text{ \AA}$), B the angular (2θ) width at half maximum intensity of the peak (rad) and θ_B is the Bragg angle of the peak.

The effect of temperature on the crystallite size is shown in Fig. 10. The interlayer spacing d_{002} was found to be around 3.6 \AA , independent of temperature. The crystallite size was $L_c = 11 \text{ \AA}$ for samples prepared at temperatures up to $800 \text{ }^\circ\text{C}$, and $L_c = 12 \text{ \AA}$ for 900 and $1000 \text{ }^\circ\text{C}$. The temperature at which the crystallite size increased from around $11\text{--}12 \text{ \AA}$ corresponds to the peak hydrogen evolution rate confirming the commencement of the graphitisation process.

5. Kinetic analysis

Measured heats of devolatilisation were used to determine the activation energies of the reactions. The reaction mechanism of coal devolatilisation is a complex phenomenon consisting of bond breaking, vaporisation and gas reformation occurring simultaneously as parallel and multiple reactions. For simplicity, it was assumed that each region was represented by an individual reaction. In reality, it is likely that several reactions take place

simultaneously. Determination of each individual heat contribution as a result of the thermal decomposition is experimentally very difficult to obtain. Furthermore, it was assumed that the reactions follow the first-order reaction mechanism.

The heats of devolatilisation were first integrated in respect with time and plotted cumulatively as a degree of reaction. The degree was set to 0 before the reaction occurred and 1 when it finished. In the case of the condensation reaction, it was assumed that it was completed by the end of the measurements. The first-order reaction, with the rate constant varying with temperature according to the Arrhenius relationship, is summarised as follows:

$$\frac{d\alpha_r}{dt} = A \exp\left(-\frac{E}{RT}\right) \alpha_r \quad (6)$$

where α_r is the degree of the reaction, A the pre-exponential factor (s^{-1}), E the activation energy (J/mol), R the gas constant and T is the temperature (K).

The logarithm of Eq. (6) yields:

$$\ln\left(\frac{d\alpha_r/dt}{\alpha_r}\right) = \ln A - \frac{E}{RT} \quad (7)$$

Finally, the left side of Eq. (7) was plotted against $1/T$. A linear trendline was fitted through each curve where the slope equals $-E/R$. The activation energies and calculated heats of pyrolysis are summarised in Table 4.

6. Modelling

There have been previous attempts to model heats of reactions of coal pyrolysis [26,28]. Suzuki and Ishida have developed a model based on the major atomic group method. This model cannot predict the rate of change of the reactions, but is useful in estimating the overall enthalpy of the system. Merrick, on the other hand, estimated the heats of reactions based on the heats of formation of the major volatile species and predicted a very strong exothermic reaction. The model can follow the rate of change of the overall reaction, however, it was later confirmed that the reactions are overpredicted [29], and the model was further corrected.

The model proposed in this work incorporates the major individual heat constituents in the overall heat of pyrolysis ΔH . The change of each heat of reaction with respect to temperature $d\Delta H_i/dT$ is described as:

$$\frac{d\Delta H_i}{dT} = \frac{\Delta H_i dW_i}{dT} \quad (8)$$

$$\frac{dW_i}{dt} = -k_{r,i} W_i \quad (9)$$

where ΔH_i is the heat of reaction (J/(m³ K)), T the temperature (K), W_i is the fraction of evolution of each reaction, t the time (s) and $k_{r,i}$ is the rate of the reaction described with Arrhenius expression:

$$k_{r,i} = A_i \exp\left(-\frac{E_i}{RT}\right) \quad (10)$$

Assembling Eqs. (8)–(10) yields:

$$\frac{d\Delta H_i}{dT} = \Delta H_i \frac{d}{dT} \left[\exp \left(- \int A_i \exp \left\{ - \frac{E_i}{RT} \right\} dt \right) \right] \quad (11)$$

Findings from the current study suggest the existence of the following major regions of activity during coal devolatilisation: dehydration, pre-plastic stage, plastic stage, secondary devolatilisation, and contraction. The most complex region, with several changes occurring at the same time, was the plastic stage. Besides the exothermic re-solidification, the endothermic tar vaporisation was also detected in this region. At lower heating rates, the heats of vaporisation of the tars were small and could be neglected, although at higher heating rates, these heats should also be considered. Accounting for the major heats of devolatilisation, the total heat change with temperature is:

$$\frac{d\Delta H}{dT} = \sum_{i=1}^5 \frac{d\Delta H_i}{dT} \quad (12)$$

where $d\Delta H_i/dT$ for $i = 1, \dots, 5$ represents the change of the individual heats of reactions with the temperature.

Individual heats and rate of reactions are summarised in Table 5. While the heat of dehydration was taken as constant for the three coals, the heats from the pre-plastic stage, plastic region, secondary devolatilisation and contraction were correlated to some known coal property. For example, the heats in the pre-plastic range were expressed as a function of carbon content, heats in the plastic range as a function of maximum fluidity, heat of secondary reaction as a function of released methane and the heat of contraction as a function of the aromatic hydrogen to carbon ratio. The latter was estimated with Eq. (13) according to van Krevelen [3].

$$\frac{H_{ar}}{C_{ar}} = \frac{H_r(1.65 - 0.04553C + 4.04 \times 10^{-4}C^2)/H}{FC/C} \quad (13)$$

where H_r is the hydrogen content in the residue at 625 °C ($\approx 2.2\%$), H the hydrogen content in the coal (%), FC the fixed carbon (%) and C is the carbon content (%).

The rates of reactions were expressed as an average of the corresponding activation energies and the pre-exponential factor calculated to fit the required peak temperature. Comparisons of the measured and predicted heats of devolatilisation for the three thermal coals are shown in Fig. 11. The model prediction shows agreement with the measured

Table 5
Heats and rates of individual reactions during coal devolatilisation

Region	ΔH_i (kJ/kg)	$k_{r,i}$
Dehydration	12	$2.35E + 17 \exp(-80000/RT)$
Pre-plastic region	$15.1C - 1245.4$	$2.90E + 13 \exp(-100000/RT)$
Plastic region	$-1.2MF - 1.357$	$2.35E + 17 \exp(-135000/RT)$
Secondary devolatilisation	$-131.7 + 45.57 X_{CH_4}$	$1.14E + 26 \exp(-220000/RT)$
Contraction	$793 - 42107H_{ar}/C_{ar}$	$22000 \exp(-65000/RT)$

R : gas constant; C : carbon content from the ultimate analysis (wt.%); MF: maximum fluidity (ddpm); X_{CH_4} : total amount of methane from mass spectrometric analysis; H_{ar}/C_{ar} : aromatic hydrogen–carbon ratio.

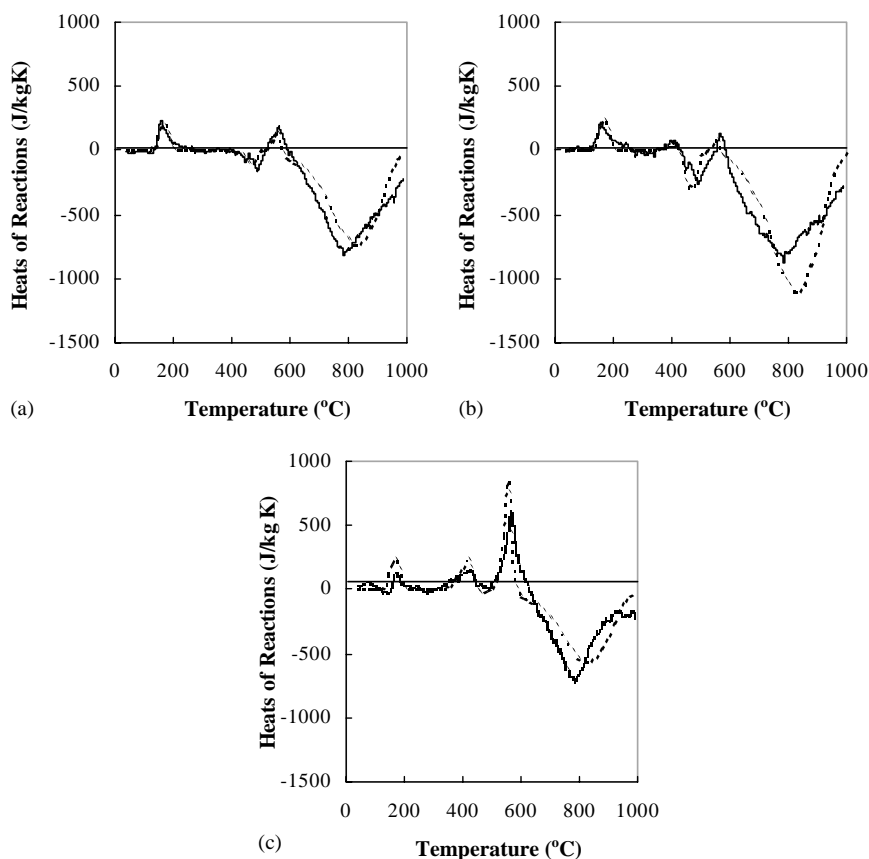


Fig. 11. Comparisons of the measured (—) and predicted (---) heats of reactions: (a) Baal Bone; (b) Drayton; (c) Moura.

data. Further modifications of the model, however, would have to be applied to cover extended range of varieties of coals and coals from different origin. In particular, it would be advantageous to also consider carbonisation behaviour and thermoplastic properties in future developments of the model. Coal devolatilisation is also known to be affected by heating rate, particle size and ambient pressure, which in this work have not been considered. Further developments in this area could be beneficial for the understanding of the thermal behaviour of coal under packed bed pyrolysing conditions.

7. Conclusions

Thermal behaviour of coals was investigated by applying computational calorimetric and gas analysis techniques. Five distinctive regions of thermal activity were detected during

the heating of coal. According to the volatiles generated and the physical transformations developed in the coal matrix, the regions were classified as dehydration, pre-plastic region, plastic region, secondary devolatilisation and contraction. The heat of dehydration was rather small and only a fraction of a percent of strongly bounded water was estimated to be present in the previously dried samples. The endothermic prepyrolytic transformation reaction was assumed to be predominant in the pre-plastic stage. The plastic stage was found to be slightly exothermic with a negligible tar vaporisation effect. The exothermicity was related to the re-solidification reaction, after which endothermic secondary devolatilisation was detected. Hydrocarbons, with methane as a major constituent, as well as water, CS₂ and H₂S were also detected in this region. The major thermal reaction commenced at 600 °C with a trough at 790 °C associated with the contraction within carbon hexagonal planes. Hydrogen was the most responsible for reformation of the stronger C–C bonds, however, CO, NH₃ and HCN were also detected in this temperature region. Measured heats of devolatilisation were used to establish the activation energies for the individual reaction. The activation energies were then incorporated in a model for predicting the heats of reactions of selected coals.

Acknowledgements

The financial support for this work was provided by the Australian Research Council and their contribution is gratefully acknowledged. We wish to express our sincere gratitude to the late Dr. J. Belton for the initiation and support of this project. We also acknowledge the contributions of Asst. Prof. V. Sahajwalla, Dr. S. Gaal and Dr. C. Wu from the University of New South Wales and their help and assistance with the XRD and MS work and Dr. E. Suuberg from Brown University for valuable discussions and advice. The TG–FTIR work was greatly assisted by the Advanced Fuel Research, CT and we are sincerely thankful to Dr. M.A. Wójtowicz and R. Bassilakis for their contribution.

References

- [1] S.C. Saxena, *Prog. Energy Combust. Sci.* 16 (1990) 55.
- [2] F.E. Ndaji, I.M. Butterfield, K.M. Thomas, *Fuel* 76 (1997) 169.
- [3] D.W. van Krevelen, *Coal Typology—Physics—Chemistry—Constitution*, Elsevier, Amsterdam, 1995.
- [4] V. Strezov, J.A. Lucas, L. Strezov, *Coke Making Int.* 14 (2002) 60.
- [5] J.-L. Yu, V. Strezov, J.A. Lucas, G.-S. Liu, T. Wall, *Proc. Comb. Inst.* 29 (2002) 467.
- [6] E. Kasai, T. Kitajima, T. Kawaguchi, *ISIJ Int.* 40 (2000) 842.
- [7] R. Cyprès, C. Soudan-Moinet, *Fuel* 60 (1981) 33.
- [8] R. Loison, *Coke Quality and Production*, Butterworths, London, 1989.
- [9] R.J. Rosenvold, J.B. Dubow, K. Rajeshvar, *Thermochim. Acta* 53 (1982) 321.
- [10] A.J. Lopez-Peinado, P.J.J. Tromp, J.A. Moulijn, *Fuel* 68 (1989) 999.
- [11] S.K. Janikowski, V.I. Stenberg, *Fuel* 68 (1989) 95.
- [12] O.P. Mahajan, A. Tomita, P.L. Walker Jr., *Fuel* 55 (1976) 63.
- [13] P.I. Gold, *Thermochim. Acta* 42 (1980) 135.
- [14] J.P. Elder, M.B. Harris, *Fuel* 63 (1984) 262.
- [15] V. Strezov, J.A. Lucas, L. Strezov, *Metall. Mater. Trans. B* 31 (2000) 1125.

- [16] V. Strezov, J.A. Lucas, L. Strezov, J. Thermal Anal. Calorim. 72 (2003) 907.
- [17] J.V. Beck, B. Blackwell, C.R. St. Clair, Inverse Heat Conduction—Ill Posed Problems, Wiley, New York, 1985.
- [18] C.J. Geankoplis, Transport Process and Unit Operations, Allyn & Bacon, Boston, 1983.
- [19] R.M. Carangelo, P.R. Solomon, D.J. Gerson, Fuel 66 (1987) 960.
- [20] J. Tomeczek, H. Palugniok, Fuel 75 (1996) 1089.
- [21] A.A. Agroskin, E.I. Goncharov, L.A. Makeev, V.P. Yakunin, Coke Chem. 5 (1970) 7.
- [22] Y. Yun, E.M. Suuberg, Fuel 72 (1993) 1245.
- [23] A.A. Agroskin, E.I. Goncharov, N.S. Gryaznov, Coke Chem. 9 (1972) 3.
- [24] H.D. Glass, Fuel 34 (1955) 253.
- [25] N. Berkowitz, W. den Hertog, Fuel 41 (1962) 507.
- [26] D. Merrick, Fuel 62 (1983) 540.
- [27] K.A. Davis, R.H. Hurt, N.Y. Yang, T.J. Headley, Combust. Flame 100 (1995) 31.
- [28] T. Suzuki, M. Ishida, Energy Dev. Jpn. 6 (1983) 279.
- [29] D. Merrick, in: A. Volborth (Ed.), Coal Science and Chemistry, Elsevier, Amsterdam, 1987, pp. 307–342.